Journal of Applied Polymer Science

Electrical, Mechanical, and Crystallization Properties of Ethylene-Tetrafluoroethylene Copolymer/Multiwalled Carbon Nanotube Composites

Yuan Rui,[1] Jiaxi Guo,[1] Jeff Harwell,[1] Tomoaki Nakanishi,[2] Seigo Kotera,[2] Brian P. Grady[1]

[1]Department of Chemical, Biological and Materials Engineering and CANTEC, University of Oklahoma, Norman, Oklahoma 73019

[2]Polymer Material Technology Function, Research Center, Asahi Glass Co., Ltd., Kanagawa-ku, Yokohama 221-8755, Japan

Correspondence to: B. Grady (E-mail: bpgrady@ou.edu)

ABSTRACT: Multiwalled carbon nanotubes (MWCNTs) were melt-mixed in a conical twin-screw extruder with a random copolymer of ethylene and tetrafluoroethylene. Surprisingly, the electrical percolation threshold of the resultant composites was quite low; ~0.9 wt %. In fact, this value is as low or lower than the value for most MWCNT/semicrystalline polymer composites made with roughly equivalent aspect ratio tubes mixed in a similar manner, for example, melt mixing. This low percolation threshold, suggestive of good dispersion, occurred even though the polymer surface energy is quite low which should make tubes more difficult to disperse. Dynamic mechanical measurements confirmed the rather low percolation threshold. The effect of nanotubes on crystallization kinetics was quite small; suggesting perhaps that a lack of nucleation which in turn reduces/eliminates an insulating crystalline polymer layer around the nanotubes might explain the low percolation threshold. Finally, the modulus increased with the addition of nanotubes and the strain at break decreased. © 2014 Wiley Periodicals, Inc. J. Appl. Polym. Sci. **2014**, *131*, 41052.

KEYWORDS: composites; copolymers; graphene and fullerenes; nanotubes

Received 5 February 2014; accepted 22 May 2014

DOI: 10.1002/app.41052

INTRODUCTION

Poly(tetrafluoroethylene) (PTFE) is well-known for being intractable to many normal polymer processing methods such as extrusion. One well-known method for maintaining some of the properties of PTFE such as its low surface energy while in turn increasing the ability to process the polymer is to copolymerize tetrafluoroethylene (TFE) with ethylene. The resulting ethylene-tetrafluoroethylene (ETFE) copolymer is melt-processible and also has the interesting property of being transparent, because of small crystal size. ETFE has excellent mechanical properties, along with being highly chemical and radiation resistant. This polymer is used in a number of applications, including the construction industry where perhaps the most high-profile use of this material was as the roofing material in the "Water-Cube" swimming complex highlighted at the Beijing Olympics.

The thermal behavior of the material is also quite interesting and complicated. In a very interesting study by Tashiro and coworkers,[1] the melting temperature of the ETFE copolymer showed a relative maximum at a molar fraction of 50 mol % of TFE repeat units and a relative minimum at 67 mol % TFE content. As the authors noted in the article, this type of relationship between melting temperature and monomer fraction is unique. This uniqueness is a result of the fact that ETFE is one of the few copolymers that has one unit cell containing both comonomers. The source of controversy stems from the unit cell; only recently has the unit cell been proven to be monoclinic[2] rather than orthorhombic[3] for example. Further, multiple researchers have reported a thermal transition at ~100°C as being a monoclinic (or orthorhombic) to hexagonal transition[4,5] although the glass transition occurs in this temperature region as well for certain copolymer compositions. In fact, the two temperatures are similar around the most common copolymer composition of equal ethylene and TFE repeat units. In dynamic mechanical spectra the distinction is clear since the glass transition feature in tan delta is much larger than that of the monoclinic to hexagonal transition.[6] In addition, Tashiro and coworkers have suggested that a small amount of a third monomer can affect the specifics of the thermal behavior substantially.[7]

To our knowledge, no studies have examined composites of these semicrystalline copolymers with carbon nanotubes. One effect of adding carbon nanotubes to a semicrystalline polymer is to increase the conductivity dramatically once a critical nanotube concentration is reached, which is termed the percolation

Table I. Representative Percolation Threshold and Change in Nonisothermal Crystallization Temperature at a Concentration at or Just Above the Percolation Threshold for Various Semicrystalline Polymers Filled with MWCNTs Prepared by Melt-Mixing[a]

Polymer	Percolation threshold (wt %)	Change in temperature (K)
Isotactic Polypropylene	0.5% (Ref. 10), 1% (Refs. 10 and 11), and 1.5% (Ref. 12)	4.4 (Ref. 11) and 8 (Ref. 12)
Polyamide 6	0.5–2–3% (Ref. 9)[b]	17 (Ref. 9)
Polyamide 6,6 (Ref. 8)[c]	1.5%	12
Polyamide 12 (Ref. 13)	1%	9
Linear Low Density Polyethylene	2.5% (Ref. 14)	
High Density Polyethylene	2.8% (Ref. 15)	4 (Ref. 16)
Polyvinylidene Fluoride (Ref. 17)	2%	4
ETFE copolymer (this article)	0.9%	1.5

[a] The temperature shift in nonisothermal crystallization temperature is not a strong function of concentration above ~1% nanotubes because the effect quickly saturates with added nanotubes. However, a consistent basis was desired for this table. In addition, the exact temperature does depend on cooling rate used; the cooling rates were not all the same but were on the order of 10°C/min.
[b] The percolation threshold depended on the mixing conditions used.
[c] The same nanotubes, mixing equipment, mixing time, and almost the same mixing speed (80 vs. 100 rpm currently) were used as was used in the current ETFE study.

threshold.[8] Another consistent effect of carbon nanotubes on most semicrystalline polymer is the nucleation of crystallinity.[9] One way to determine whether a solid nucleates crystallinity is to see if the crystallization temperature increases when a polymer is cooled from the melt state at a constant rate. Table I shows the percolation threshold and change in crystallization temperature at a concentration just above the percolation threshold for some common semicrystalline polymers. The polyamide 6,6 study listed in Table I used the same nanotubes and analogous experimental procedures as was used in this study and provide a very good direct comparison to the results presented in this article.

The purpose of this study is to investigate the properties of a commercial ETFE copolymer that was melt-mixed with nanotubes. The electrical percolation threshold, 0.9 wt %, is low for a semicrystalline polymer prepared by melt-mixing and the plateau electrical resistivity is also low. Both were expected to be much higher given the low surface energy of the polymer, which was thought would yield poorly dispersed tubes. Unlike with most semicrystalline polymers where nanotubes are strong nucleators of crystallinity, crystallization kinetics as measured by the crystallization temperature in nonisothermal experiments were hardly affected. As was seen previously with polyamide 6,6 but otherwise has not been reported to our knowledge, the glass transition temperature (T_g) as measured by dynamic mechanical thermal analysis (DMTA) and that measured by differential scanning calorimetry (DSC) did not change consistently with the addition of nanotubes; the former decreased with the addition of nanotubes while the latter increased. The modulus increased with the addition of nanotubes, the strain at break decreased and the tensile strength decreased slightly with added nanotubes and then was constant.

MATERIAL AND METHODS

Materials

Ethylene tetrafluoroethylene (ETFE) pellets provided by Asahi Glass Company were used. This ETFE is a copolymer, contains ~50% TFE comonomer, and has a melt flow rate of 33 g/10 min according to ASTM D 3159. The melting temperature of the pure polymer was measured at 256°C, which indicates, according to the melting temperature-composition plot in Ref. 1, that the composition was between 45 and 50% ethylene. SMW^{TM}-100 CNTs with an average aspect ratio of 94 (average length = 735 nm, average diameter = 7.8 nm) were provided by Southwest Nanotechnologies; the number distribution for length is given in a previous article from our group.[18] Most commercial nanotubes have an aspect ratio between 50 and 150; hence, these nanotubes can be considered to have an aspect ratio characteristic of most commercial nanotubes.[18]

Composite Preparation

The desired amount of carbon nanotubes and ETFE pellets were added to a DSM Xplore^{TM} twin-screw microcompounder with corotating screws. Composites were mixed at a rotation speed of 100 RPM and 270°C for 3 min. All samples were prepared under a nitrogen blanket to minimize degradation. The extruded strands were cut into pellets and compression molded in a Carver Laboratory Press where they were heated to 280°C and held under a pressing force of 45 kN for 10 min. The sheets were then cooled to 100°C under compression by directing a fan at the hot plates; the cooling time was around 30 min.

Conductivity Measurements

The electrical conductivities of low conducting samples (resistivities' $> 1 \times 10^7$ ohm-cm) were measured with an Agilent 4339B high resistance meter and 16008B resistivity cell. Composite films of dimensions 63.5 × 63.5 × 0.33 mm^3 were tested under at least three different voltages to obtain an average resistivity, which was then converted to the conductivity. The conductivites of moderately conducting samples (resistivities $< 1 \times 10^7$ ohm-cm) were measured using a four-point probe geometry as outlined in the American Standard for Testing and Materials (ASTM) Standard D 4496. Copper electrodes were attached to rectangular pieces of composite films with conductive silver epoxy (MG Chemicals 8331). The samples were then attached

to a Keithley 2000 multimeter, which measured the resistance of the sample, from which the resistivity and conductivity were calculated based on the dimensions of the sample. Only one sample was measured per concentration.

Dynamic Mechanical Analysis

DMTA was performed with a Rheometric Scientific RSA II to measure loss and storage moduli as a function of temperature. Measurements were taken on compression molded samples that were ~30 mm long and 5 mm wide at 1 Hz frequency and 4°C temperature steps. Glass transition temperatures were calculated by determining the temperature corresponding to the maximum value of tan delta in the glass transition temperature region.

Tensile Tests

Tensile tests were performed using a United STM-2K tensile tester at an elongation rate of 1.3 cm per minute. Compression molded films were cut using an ASTM-D-1708 die from Dewes-Gumbs on a manual expulsion press. At least seven replicates were done on samples at every nanotube content level.

Nonisothermal Crystallization and Melting

DSC measurements were performed using a TA Instruments Q-1000 Calorimeter. Samples of 10–15 mg were cut from compression molded films and crimped in standard aluminum pans. Temperature calibration was performed during heating using indium, tin, and biphenyl, and heat capacity calibration was performed with sapphire. Samples were heated to 320°C, held for 5 min, then cooled to −80°C at 10°C/min and held for 5 min (referred to as the cooling run), and then heated to 320°C at 10°C/min (referred to as the heating run). The temperature corresponding to the maximum in heat evolution was recorded as the crystallization temperatures. Upon heating, the midpoint method was used to determine the glass transition temperature while the melting temperature was assigned as the temperature corresponding to the maximum heat influx within the crystal-to-melt transition. As noted previously, there is some controversy regarding the designation of this transition as a glass transition. The appearance of this feature, shown in Figure 1, does suggest a step change in heat capacity, which is consistent with the glass transition temperature, but also there is a peak which could be enthalpy relaxation or a contribution from a structural transition.

Small-Angle X-ray Scattering Measurements

Small-angle x-ray scattering measurements were made in transmission with a SMax-3000 from Rigaku equipped with a CuKa source and a 10 × 10 cm^2 2-D wire detector placed ~150 cm from the sample position. Silver behenate was used to determine the exact pixel to q ($q = 4\pi\sin\theta/\lambda$; $\theta = 0.5 \times$ scattering angle, λ = 1.54 Å) conversion.

Microscopy

For both transmission electron microscopy (TEM) and optical microscopy, thin sections of samples from the various composites were cut using a microtome. TEM experiments were carried out on a JEOL 2000-FX 200 kV TEM. Transmission optical micrographs according to the standard ISO 18553 were collected with a Leitz Dialux 20 Photomicroscope equipped with an Olympus DP71 microscope digital camera. Agglomerate size distribution

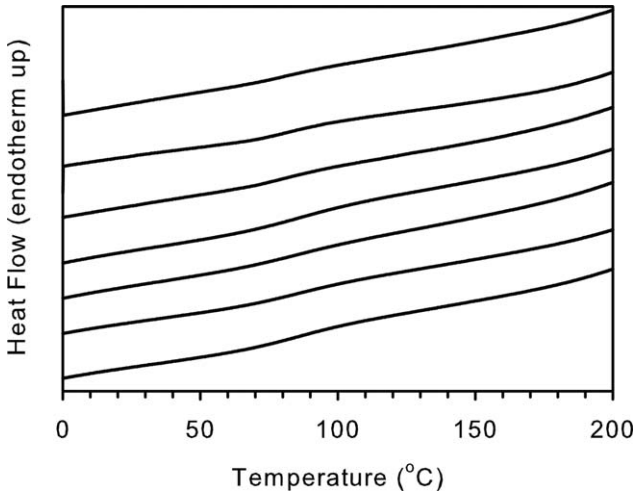

Figure 1. Raw DSC curves during heating at 10°C/min after cooling at 10°C/min expanded in temperature to focus on the glass transition region. From bottom to top are nanotube contents (wt %) of 0, 0.5, 1, 2, 3, 4, and 5%. Curves are offset vertically to enhance presentation quality.

via circle-equivalent diameters was used to determine the area ratio from the images using the image analysis software ImageJ Version by calculating the ratio of multiwalled carbon nanotube (MWCNT) agglomerate area to the total area of the image. Only agglomerates with circle-equivalent diameters larger than 5 μm were considered as agglomerates in calculating this ratio as according to ISO 18553. At least 10 images of the type shown in Figure 9 were used to calculate size distributions for each nanotube content. For scanning electron microscopy, samples were fractured after freezing in liquid nitrogen; the fracture surface was coated with a ~4 nm layer of iridium and a Zeiss NEON High Resolution SEM was used to capture images.

RESULTS AND DISCUSSION

Bulk conductivity measurements as a function of mass fraction of added nanotubes are shown in Figure 2. The solid curve shown is the best least-squares fit to the power law represented by eq. (1)[19]:

$$\sigma(p) = B(p - p_c)^t \quad (1)$$

This equation contains the experimental conductivity value $\sigma(p)$ for concentrations $p > p_c$, the proportionality constant B (=0.1 S/cm), the electrical percolation threshold p_c (=0.9 wt %) and the critical exponent t (=2). Mechanistically, this dependence of conductivity on loading arises because a continuous carbon nanotube network must form before conductivity can increase dramatically. The continuous network does not imply that carbon nanotubes are touching one another; electrons can hop from one nanotube to another if the nanotubes are close enough due to quantum tunneling effects. A percolation threshold of 0.9 wt % is rather low for a semicrystalline polymer that has been melt-mixed with MWCNTs, as Table I demonstrates. This result is suggestive of good dispersion of the tubes in the polymer; at least in a nanometer sense. If only micron-size clumps were present (see Figure 8), the conductivity would be poor. To achieve high conductivity requires a

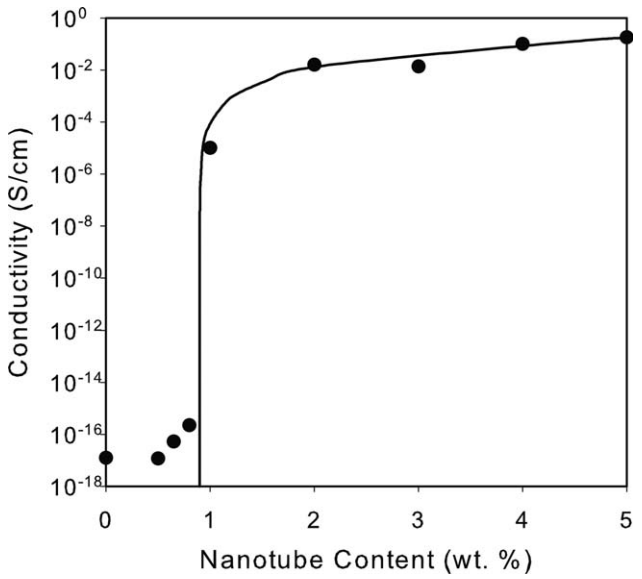

Figure 2. Conductivity for ETFE filled with MWCNTs. Dots represent the data while the line represents the best fit result according to eq. (1).

significant concentration of individual (or aggregates with small number of tubes in each aggregate) tubes to achieve percolation at low conductivities; such tubes are present as shown in the

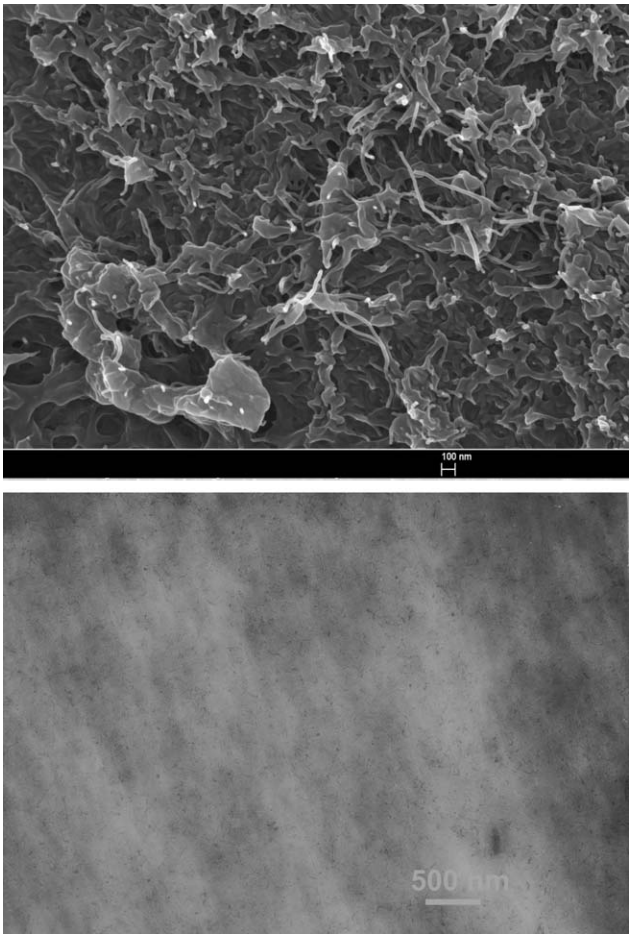

Figure 3. Scanning electron micrograph (top) and transmission electron micrograph (bottom) for ETFE filled with 4 wt % MWCNTs.

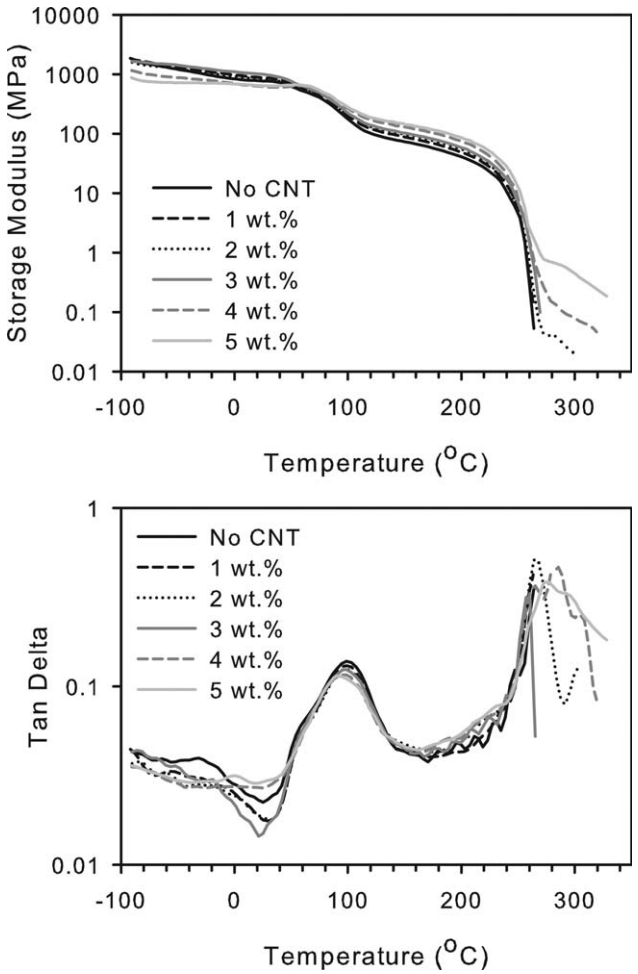

Figure 4. Storage modulus (top) and tan delta (bottom) for ETFE filled with MWCNTs.

micrographs presented in Figure 3. After tubes are well-dispersed in this nanoscale sense aggregation can occur; micron-scale inhomogeneity due to this aggregation should be beneficial since a conducting network can form at lower nanotube loadings. This phenomena is almost certainly why annealing nanotube composites can lead to orders-of-magnitude increases in conductivity.[20,21] Such type of network structure is not obvious from the electron micrographs, but determining whether a network has formed from micrographs has not been found to be practically feasible.

As another measure of the good dispersion of the nanotubes, a comparison of conductivity vs. percolation threshold done in a review article[22] correlated these two measures with dispersion. A plateau conductivity of 10^{-1} S/cm and percolation threshold of 0.9% suggests tubes that are very conductive and dispersed well in ETFE. The conductivity at 5 wt %, that is, well above the percolation threshold, is an order of magnitude higher in this copolymer than in a composite with an equal concentration of the same tubes mixed into polyamide 6,6[8] using the same equipment.

Dynamic mechanical spectra are shown in Figure 4. The peak in tan delta at ~100°C is attributed to the glass transition of the

ETFE polymer.[6] The temperature corresponding to the relative maximum of the glass transition decreased with increasing nanotube concentration; this behavior will be explored more fully when discussing DSC data. The height of the T_g tan delta peak looks to decrease slightly with temperature. A decrease in the height of this peak indicates that a smaller amount of material is participating in the glass transition; however, this decrease is quite small and hence this effect is quite minimal. A shoulder centered at ~50°C appears on this main peak, and is attributed to a change in crystal structure as described earlier.[6] Because of the weakness of this transition, no change in this peak's characteristics can be attributed to the presence of nanotubes. The β transition centered at about −40°C clearly decreased in magnitude and shifts to higher temperature with the addition of nanotubes; very little is known about this transition except that it also has been attributed to a crystalline relaxation.[6] In fact, one study[23] found two peaks in tan delta in this temperature region; the frequency of that experiment, 3.5 Hz, was almost the same as the conditions used in the current study. However, the torsional pendulum geometry was very different from the tensile geometry used here.

The storage modulus E' showed a measurable rubbery modulus above the melting temperature of the polymer; a feature that has been noted elsewhere by our group in nanotube-filled composites.[8,10,24] The reason for this behavior is that the nanotubes cause the formation of a network which is able to support a stress unlike a molten polymer. A percolation threshold can be defined using this measurement as the concentration where the rubbery modulus increases with nanotube concentration as is done with linear viscoelastic measurements in shear[25] and the value was between 1 and 2% (no plateau was seen at 3% NT content because the sample broke prematurely). The fact that the electrical percolation threshold was lower than the rheological percolation threshold is not common[24,26–31] but not unheard of either.[32,33]

Results for tensile properties are found in Figure 5. The modulus showed an increase with the addition of nanotubes; the qualitative shape of the curve does not match that of the heat of fusion. Hence, nanotubes are having a positive reinforcing effect on the composite. The tensile strength decreases and then reaches a plateau with added nanotubes while the strain at break decreases monotonically with added nanotubes in an exponential-type fashion, which has been noted elsewhere.[18]

Figure 6 shows the change in crystallization temperature with the addition of nanotubes. The crystallization temperature increased, but only very slightly relative to other semicrystalline polymers as shown in Table I. The conclusion from this measurement is that the nucleation effect is not very strong; for example, the overall crystallinity versus time is only very slightly affected with the addition of nanotubes. Isothermal crystallization experiments, which would provide additional quantitative comparison in terms of the rate, were not attempted because of previous reports that cooling rates cannot be fast enough to prevent crystallization during cooling.[34] The fractional crystallinity dropped only slightly with the addition of nanotubes, roughly linearly from 25 to 24% from 0–5 wt % tubes. Such a drop is only outside of experimental error because of the consistency of the change from low to high nanotube contents.

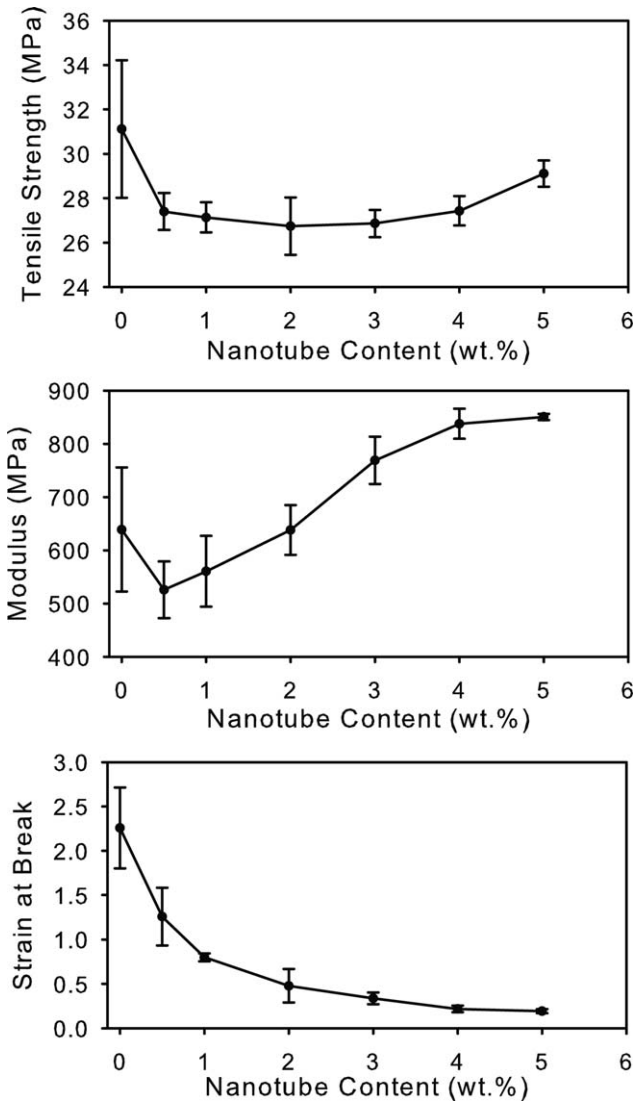

Figure 5. Tensile strength, Young's modulus, and strain at break (top to bottom) for ETFE filled with MWCNTs.

In our opinion, the rather low percolation threshold for ETFE as compared to the polyamide 6,6 (which was done with almost exactly the same procedure) is due to the rather weak nucleation effect. Morphologically, a nanotube that nucleates crystal growth will have crystals that are surrounding the tube, which in turn act as a coating not allowing for nanotube-nanotube contact. One possibility for the weak dependence was that only some nanotubes nucleated crystallinity while others did not; we view this possibility as unlikely since to our knowledge no nanotube characteristics, other than surface chemistry, have been shown to significantly affect nucleation ability. A more likely explanation was that the crystalline film coating the nanotubes is of approximately uniform thickness and/or was more patchy than is typically found for most nanotube-filled semicrystalline polymers. In other words, in ETFE, non-nanotube nucleation sites more effectively compete with nanotube nucleation sites than is typical for a nanotube-filled polymer.

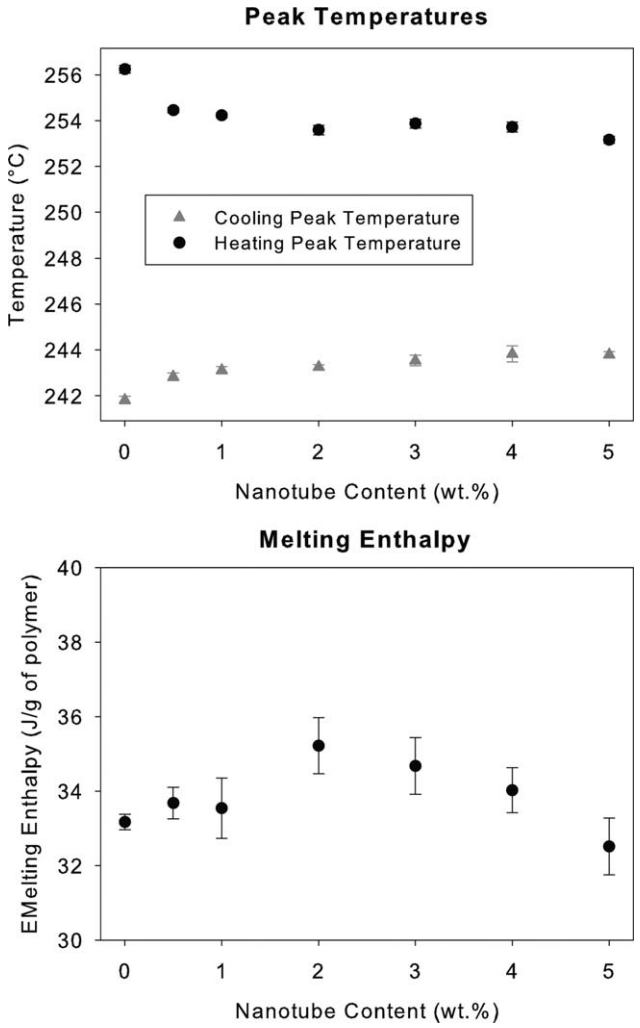

Figure 6. Nonisothermal crystallization temperature, melting temperature (top) and melting enthalpy (bottom) for ETFE filled with MWCNTs.

Although we do not believe the cause of the low percolation threshold was better dispersion, the torque measured in the DSM mixer was about a factor of two higher for the ETFE versus polyamide 6,6. Hence, we cannot absolutely rule out a higher viscosity as leading to better dispersion, which in turn leads to a smaller percolation threshold, although surface energy considerations still strongly do not favor a better dispersion in ETFE copolymers. Finally, a third possibility is that nanotubes were broken less in the ETFE vs. the polyamide 6,6; with a higher viscosity and the same equipment, mixing time and a higher mixing speed (100 rpm currently vs. 80 rpm with polyamide 6,6), such a result is extremely unlikely.

The melting temperature decreased slightly with the addition of nanotubes as well. Typically in semicrystalline polymers, the melting temperature decreases with the addition of nanotubes, which is due to the change in nucleation rate causing the formation of thinner crystals. Of course, the decrease here could be a result of decreasing thickness. However, with ETFE, if a particular copolymer is more likely to be nucleated by nanotubes, then the crystallization temperature

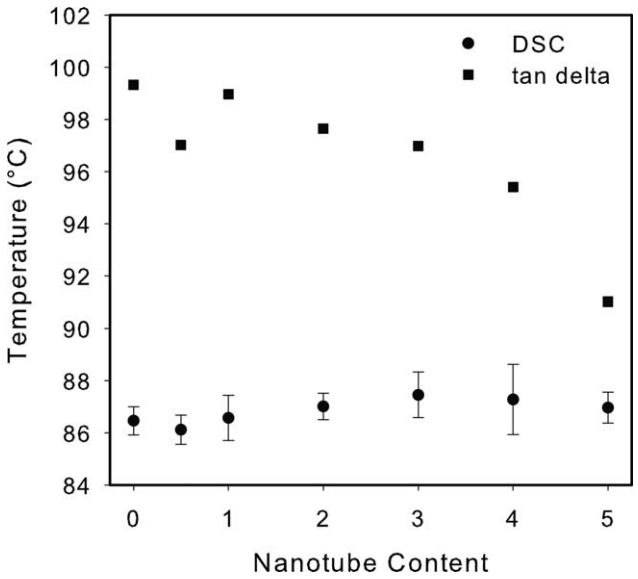

Figure 7. Glass transition temperature for ETFE filled with MWCNTs.

could be changed since the crystallization temperature in ETFE depends strongly on the composition of the copolymer.[1] As noted previously, the enthalpy of fusion increased with increasing nanotube content suggesting that the fractional crystallinity also increased. We are not aware of an appropriate value to use for the enthalpy corresponding to melting of a single crystal, so we cannot calculate percent crystallinity. As was found here, changes in melting temperature and fractional crystallinity are small with the addition of nanotubes in most semicrystalline polymers.

The glass transition temperature was measured by both DSC and DMTA and the results are shown in Figure 7. T_g showed a decrease in value in DMTA with the addition of nanotubes, and an increase via DSC; this seemingly contradictory behavior was found previously for polyamide 6,6.[8] However as noted earlier, with ETFE we cannot be sure that the DSC transition was solely due to the glass transition. The

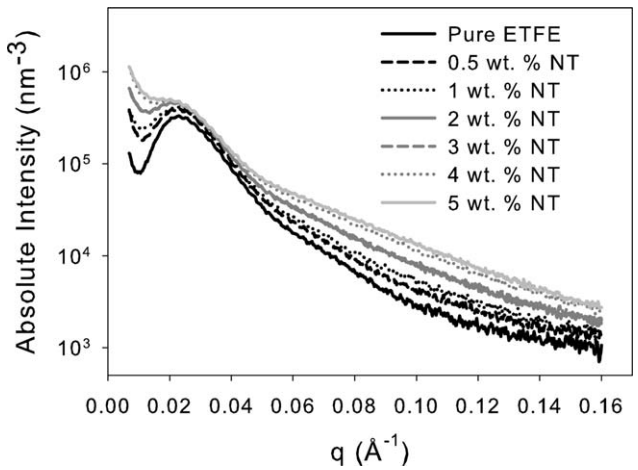

Figure 8. Small-angle X-ray scattering patterns for ETFE filled with MWCNTs.

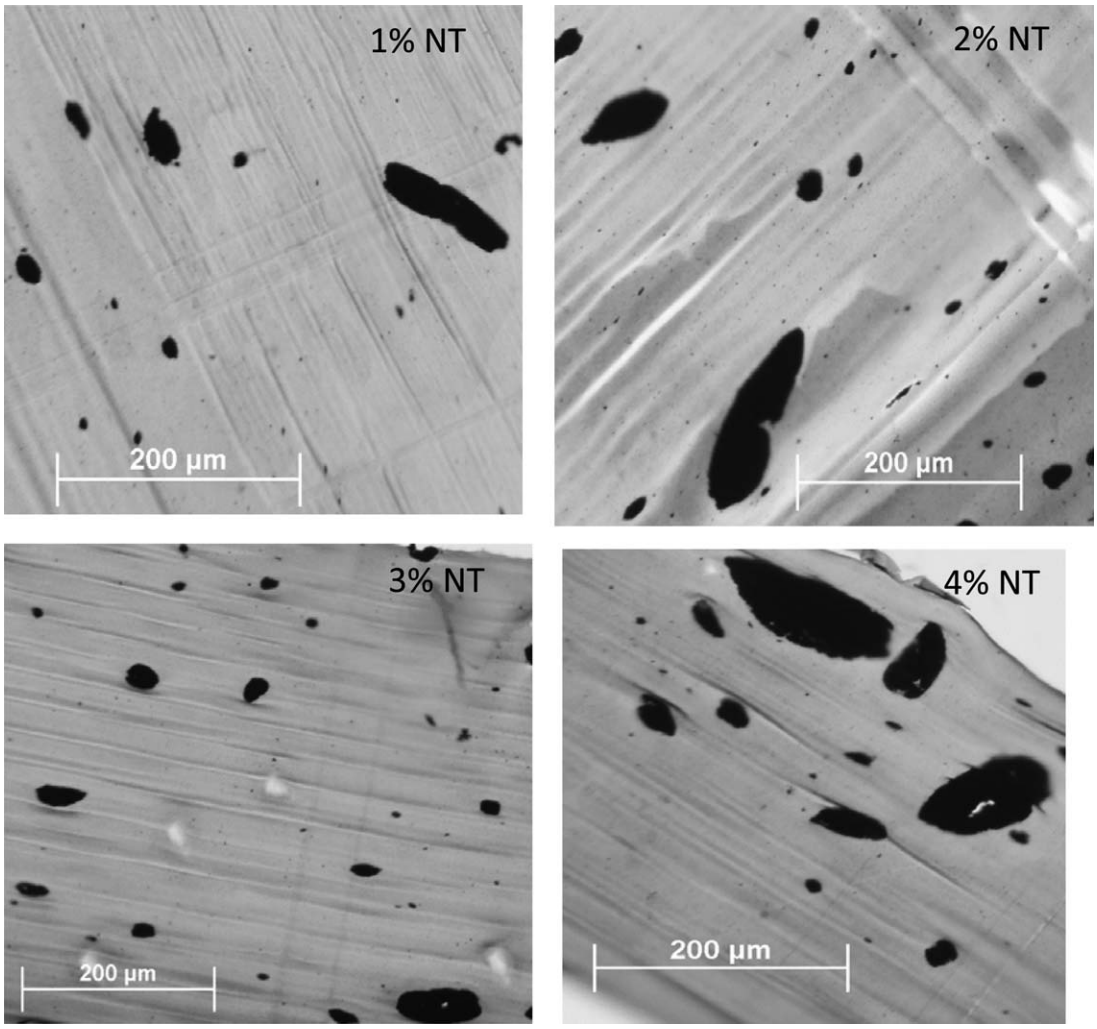

Figure 9. Optical micrographs of thin film microtomed sections of melt-mixed ETFE composites.

magnitude of the increase in T_g with DSC is much smaller in this study than in the polyamide 6,6 study. To our knowledge, only these two studies show qualitatively different T_g DSC and DMTA trends, although not very many studies have made both measurements for semicrystalline polymers. In amorphous polymers, to our knowledge, the two T_g measurements always agree in a relative sense. Our previous interpretation[8] was that the nucleation of crystallinity changes the morphology of crystallites, which in turn changes the mechanical response to the glass transition; with a presumably much weaker nucleation effect such an explanation is not as favored and it is difficult to rationalize the substantial decrease in DMTA T_g with added nanotubes.

Figure 8 shows the results from SAXS measurements. The increase in overall scattered intensity is due to the introduction of nanotubes; such increases are typically found with the addition of nanotubes.[35,36] Within the ability to distinguish shifts in peak position, no changes in the peak position occurred with the addition of nanotubes and hence the long spacing was also unchanged. The same invariance to the long spacing with the addition of nanotubes has also been found for high-density polyethylene[37] although changes were found for polypropylene[38] as well as for poly(ethylene oxide) with surfactant-stabilized nanotubes.[39]

Figure 9 shows representative optical micrographs for selected nanotube contents, and Figure 10 shows the statistical distribution of the sizes based on circle-equivalent diameters using micrographs of the type shown in Figure 9. As indicated by the text box in Figure 10, the area percentage of agglomerates >5 microns scaled approximately linearly with nanotube content, except for the 3% sample, which clearly does not follow the trend. We have no explanation for this behavior except to note that 20 different micrographs were measured for the 3% sample to reduce the possibility that the anomalous behavior was due to statistical variation. Comparing to literature values with different semicrystalline polymers, a 2 wt % Nanocyl^{TM} NC7000 in isotactic polypropylene had an area ratio of 3.1% with a percolation threshold of 0.5 wt %[10] while a 2 wt % Nanocyl^{TM} NC7000 in linear low density polyethylene had an area ratio of 3.4% and percolation threshold of 2.5 wt %.[14] Coupled with the results in this article of 3.7 and 0.9 wt %, respectively, these results show that agglomerate area is not the dominant factor in determining percolation threshold.

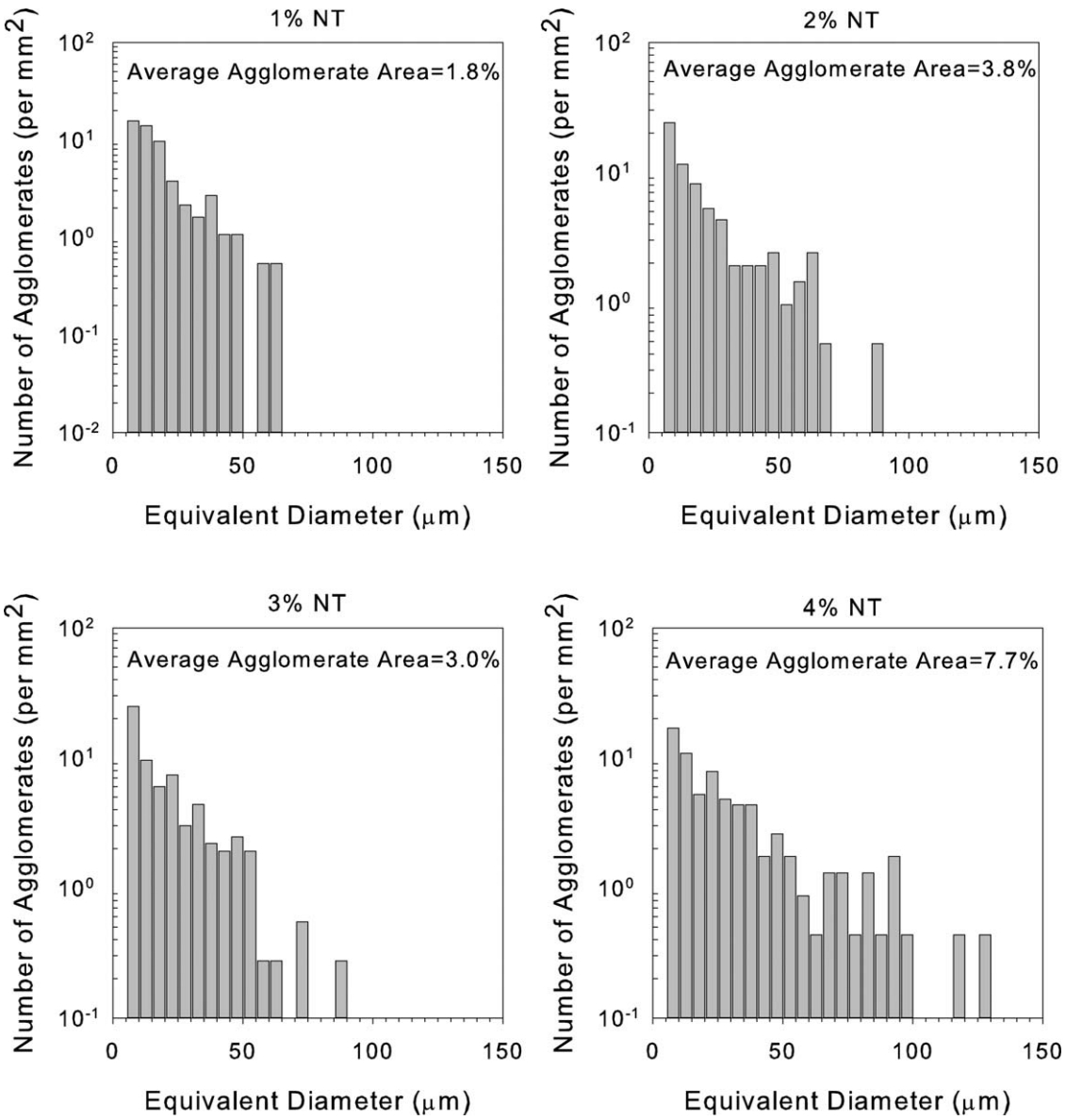

Figure 10. Distribution of frequency for agglomerates of various equivalent diameter sizes for the various composites.

CONCLUSIONS

An ETFE copolymer was mixed with carbon nanotubes and the percolation threshold was extremely low for a semicrystalline polymer, especially considering the low surface energy of the polymer. The ability of nanotubes to nucleate ETFE crystallinity was quite limited compared to the ability of nanotubes to nucleate crystallinity in other polymers, which possibly was the reason for the very low percolation threshold. The addition of nanotubes also lowered the T_g as measured by DMTA and increased the T_g as measured by DSC (although with the latter it is not clear that only T_g was being measured). At the highest nanotube content, the modulus increased by about 25%, which could not be explained by a change in crystalline fraction indicating the nanotubes were increasing the stiffness of the polymer.

ACKNOWLEDGMENTS

The authors would like to thank the Asahi Glass Company for their support of this research. BPG acknowledges a grant to support nanotube research from the Department of Energy (Grant no. ER64239 0012293). The authors would also like to thank Dr. Jiaxi Guo for his assistance, especially with electron microscopy measurements.

REFERENCES

1. Arai, K.; Funaki, A.; Phongtamrug, S.; Tashiro, K. *Polymer* **2010**, *51*, 4831.
2. Funaki, A.; Phongtamrug, S.; Tashiro, K. *Macromolecules* **2011**, *44*, 1540.
3. Tanigami, T.; Yamaura, K.; Matsuzawa, S.; Ishikawa, M.; Mizoguchi, K.; Miyasaka, K. *Polymer* **1986**, *27*, 999.

4. Tanigami, T.; Yamaura, K.; Matsuzawa, S.; Ishikawa, M.; Mizoguchi, K.; Miyasaka, K. *Polymer* **1986**, *27*, 1521.
5. Radice, S.; DelFanti, N.; Zerbi, G. *Polymer* **1997**, *38*, 2753.
6. Arai, K.; Funaki, A.; Aida, S.; Phongtamrug, S.; Tashiro, K. *J. Appl. Polym. Sci.* **2009**, *114*, 1710.
7. Funaki, A.; Arai, K.; Aida, S.; Phongtamrug, S.; Tashiro, K. *Polymer* **2008**, *49*, 5497.
8. Caamano, C.; Grady, B.; Resasco, D. E. *Carbon* **2012**, *50*, 3694.
9. Krause, B.; Pötschke, P.; Häussler, L. *Compos. Sci. Technol.* **2009**, *69*, 1505.
10. Müller, M. T.; Krause, B.; Kretzschmar, B.; Pötschke, P. *Compos. Sci. Technol.* **2011**, *71*, 1535.
11. Abbasi, S.; Derdouri, A.; Carreau, P. *J. Polym. Eng. Sci.* **2011**, *51*, 992.
12. Bao, H. D.; Guo, Z. X.; Yu, J. *Chin. J. Polym. Sci.* **2009**, *27*, 393.
13. Socher, R.; Krause, B.; Hermasch, S.; Wursche, R.; Pötschke, P. *Compos. Sci. Technol.* **2011**, *71*, 1053.
14. Müller, M. T.; Krause, B.; Pötschke, P. *Polymer* **2012**, *53*, 3079.
15. Liu, F.; Zhang, X. B.; Li, W. C.; Cheng, J. P.; Tao, X. Y.; Li, Y.; Sheng, L. *Compos. A* **2009**, *40*, 1717.
16. Mai, F.; Wang, K.; Yao, M. J.; Deng, H.; Chen, F.; Fu, Q. A. *J. Phys. Chem. B* **2010**, *114*, 10693.
17. Kang, D. J.; Pal, K.; Bang, D. S.; Kim, J. K. *J. Appl. Polym. Sci.* **2011**, *121*, 226.
18. Castillo, F. Y.; Socher, R.; Krause, B.; Headrick, R.; Grady, B. P.; Prada-Silvy, R.; Pötschke, P. *Polymer* **2011**, *52*, 3835.
19. Grady, B. P. Carbon Nanotube-Polymer Composites: Manufacture, Properties and Applications; Wiley: New York, **2011**.
20. Alig, I.; Skipa, T.; Lellinger, D.; Pötschke, P. *Polymer* **2008**, *49*, 3524.
21. Alig, I.; Lellinger, D.; Engel, M.; Skipa, T.; Pötschke, P. *Polymer* **2008**, *49*, 1902.
22. Bauhofer, W.; Kovacs, J. Z. *Compos. Sci. Technol.* **2009**, *69*, 1486.
23. Kostov, G.; Nikolov, A.; Atanassov, A. *J. Appl. Polym. Sci.* **2001**, *81*, 2626.
24. Ha, M. L. P.; Grady, B. P.; Lolli, G.; Resasco, D. E.; Ford, W. T. *Macromol. Chem. Phys.* **2007**, *208*, 446.
25. Abbasi, S.; Carreau, P. J.; Derdouri, A.; Moan, M. *Rheologica Acta* **2009**, *48*, 943.
26. Du, F. M.; Scogna, R. C.; Zhou, W.; Brand, S.; Fischer, J. E.; Winey, K. I. *Macromolecules* **2004**, *37*, 9048.
27. Hu, G. J.; Zhao, C. G.; Zhang, S. M.; Yang, M. S.; Wang, Z. G. *Polymer* **2006**, *47*, 480.
28. Lee, J. I.; Yang, S. B.; Jung, H. T. *Macromolecules* **2009**, *42*, 8328.
29. Bangarusampath, D. S.; Ruckdaschel, H.; Altstadt, V.; Sandler, J. K. W.; Garray, D.; Shaffer, M. S. P. *Polymer* **2009**, *50*, 5803.
30. Yu, S. Z.; Wong, W. M.; Hu, X.; Juay, Y. K. *J. Appl. Polym. Sci.* **2009**, *113*, 3477.
31. Kalgaonkar, R. A.; Jog, J. P. *Polym. Int.* **2008**, *57*, 114.
32. Kim, J.; Hong, S. M.; Kwak, S.; Seo, Y. *Phys. Chem. Chem. Phys.* **2009**, *11*, 10851.
33. Chatterjee, T.; Yurekli, K.; Hadjiev, V. G.; Krishnamoorti, R. *Adv. Funct. Mater.* **2005**, *15*, 1832.
34. Kostov, G.; Bogdanov, B.; Nikolov, A. *J. Therm. Anal.* **1994**, *41*, 925.
35. Buffa, F.; Abraham, G. A.; Grady, B. P.; Resasco, D. *J. Polym. Sci. Part B: Polym. Phys.* **2007**, *45*, 490.
36. Grady, B. P.; Arthur, D. J.; Ferguson, J. *Polym. Eng. Sci.* **2009**, *49*, 2440.
37. Castillo, F. Y.; Grady, B. P. *Polym. Eng. Sci.* **2012**, *52*, 1761.
38. Causin, V.; Yang, B. X.; Marega, C.; Goh, S. H.; Marigo, A. *Eur. Polym. J.* **2009**, *45*, 2155.
39. Chatterjee, T.; Lorenzo, A. T.; Krishnamoorti, R. *Polymer* **2011**, *52*, 4938.